A predictive fatigue life model for anodized 7050 aluminium alloy

Michel Chaussumier, Catherine Mabru, Majid Shahzad, Rémy Chieragatti, Farhad Rezai-Aria

HAL Id: hal-00796820

https://hal.science/hal-00796820

Submitted on 5 Mar 2013

A predictive fatigue life model for anodized 7050 aluminium alloy

Michel Chaussumier [a,*], Catherine Mabru [a], Majid Shahzad [a], Rémy Chieragatti [a], Farhad. Rezai-Aria [b]

[a] Université de Toulouse; INSA, UPS, EMAC, ISAE; ICA (Institut Clément Ader), 10 Av. Edouard Belin, 31055 Toulouse Cedex 4, France
[b] Université de Toulouse; INSA, UPS, EMAC, ISAE; ICA (Institut Clément Ader), Route de Tiellet, 81000 Albi, France

ABSTRACT

The objective of this study is to predict fatigue life of anodized 7050 aluminum alloy specimens. In the case of anodized 7050-T7451 alloy, fractographic observations of fatigue tested specimens showed that pickling pits were the predominant sites for crack nucleation and subsequent failure. It has been shown that fatigue failure was favored by the presence of multiple cracks. From these experimental results, a fatigue life predictive model has been developed including multi-site crack consideration, coalescence between neighboring cracks, a short crack growth stage and a long crack propagation stage. In this model, all pickling pits are considered as potential initial flaws from which short cracks could nucleate if stress conditions allow. This model is built from experimental topography measurements of pickled surfaces which allowed to detect the pits and to characterize their sizes (depth, length, width). From depth crack propagation point of view, the pickling pits are considered as stress concentrator during the only short crack growth stage. From surface crack propagation point of view, machining roughness is equally considered as stress concentrator and its influence is taken into account during the all propagation stage. The predictive model results have been compared to experimental fatigue data obtained for anodized 7050-T7451 specimens. Predictions and experimental results are in good agreement.

1. Introduction

Aluminum alloys 2xxx and 7xxx are extensively used in aeronautical industry due to their high strength and low density. The natural oxide layer that developed at the surface of these alloys is not thick enough to ensure a good protection of the structures in severe environment conditions. In order to increase the thickness of the oxide layer, aluminum alloy parts are often anodized. Anodization is an electrolytic process that produces amorphous aluminum oxide on the surface [1]. The benefits obtained for wear and corrosion resistance is obtained at the expense of fatigue resistance [2–5]. Numerous researchers have attributed the fatigue resistance decrease to the brittle and porous nature of the oxide layer and equally to the tensile residual stress induced during anodizing process [4,6–8]. Some others have shown that surface degradation was responsible too [9–12]. This degradation is generated principally by pickling process realized before anodic oxidation. Pits are created during pickling process as a result of dissolution of inter-metallic particles at the surface or dissolution of aluminum matrix at the interface matrix/particles [13–15]. This fatigue resistance decrease is explained by the formation of these numerous pits that facilitate crack nucleation and lead to multicrack failure [16–18].

For machined parts subjected to fatigue, it is generally accepted that the surface influence recovers three aspects: metallurgical, mechanical and geometrical. The first aspect consists principally in microstructure and in hardening due to machining; the second aspect concerns the residuals stresses induced by machining. The third aspect is then principally related to surface roughness. In the case of aluminum alloy 7010, it has been shown that fatigue resistance was principally influenced by machining surface roughness, compared to residual stresses or hardening [19,20]. This influence was confirmed for 7010 anodized cases but this effect is modified by the presence of pickling pits and anodic coating: for higher roughness, the effect of anodization on fatigue life is less important than for low roughness [21,22].

In a previous study [23], and in order to predict fatigue life of anodized 7010 aluminum alloy parts, an analytical fatigue life model has been developed which was based on Suraratchaï's model [20]. Suraratchaï's model is based on crack propagation including the stress concentration effect generated by surface roughness. This effect is defined through a local stress concentration coefficient which interacts with local stress concentration due to the presence of inclusions. Influence of inclusion is implicitly considered through the fatigue strength of the studied material. Surface roughness stress concentration coefficient is calculated using a finite element model built from roughness profiles [24]. In the study concerning anodized 7010 aluminum alloy, two surface roughness levels have been chosen (0.8 and 3.2 μm). Experimental fatigue tests have

---

shown that pickling process was very detrimental to fatigue resistance comparing to anodic oxidation process. The aim of this previous study [23] was to extend Suraratchaï's model to consider the stress concentration generated by pickling pits and the influence of the numerous pits. That was done by extending the initial model using a surface topography modeling and introducing multi crack initiation sites so that a step by step crack propagation calculation with intermediate coalescence conditions controls was necessary; a short crack growth law was also introduced to consider the higher crack growth rate according to literature. Fatigue life predictions for only pickled surface were balanced to experimental data and a good agreement has been observed.

In the current study, the fatigue behavior of 7050-T7451 aluminum alloy anodized in chromic acid bath has been investigated in order to define the respective influence of the different step of surface treatment, including machining step, pickling and anodizing ones. Specimens have been tested in four-point bending fatigue. Before fatigue testing, the surface topography of several specimens has been measured using a profilometer. Fatigue mechanisms have been identified using fractographic observations on machined, pickled and anodized specimens. EDS analysis during SEM observations has been used to characterize pits responsible for crack initiation [25]. Then, according to experimental observations, and in order to predict fatigue life of chromic acid anodized 7050 aluminum alloy structures, the analytical model of crack propagation previously developed during study on 7010 [23], and resumed above, has been re-used and developed to alloy fatigue life predictions for anodized conditions. The numerous nucleation sites match with the pickling pits identified on the surface of pickled specimens using topography measurements. The stress concentration factor at the bottom of each pit is calculated using three-dimensional finite elements models built from these topography measurements. The stress concentration factor generated by surface machining roughness is calculated using a two-dimensional finite element model built from roughness profiles measurements on machined surfaces [20,24]. Among influences of neighboring cracks, only coalescence has been considered when the plastic zones at the crack tips reach one each other. Fatigue crack propagation calculation is stopped when critical stress intensity factor is reached for one of these cracks.

2. Experimentation

2.1. Material

The material investigated in this work is 7050-T7451 aluminum alloy. Chemical composition is given in Table 1. It was provided in rolled plate form of 70 mm thickness. Metallographic analysis of the microstructure revealed that it is composed of recrystallized grains (mean size about 25–30 μm) and unrecrystallized which are highly elongated in the rolling direction as shown in Fig. 1. Three types of inter-metallic particles were mainly found in this material: Al_2CuMg, Al_7Cu_2Fe Mg_2Si particles. These particles were principally located in recrystallized grains. The average size of these particles varied between 8 and 12 μm. Mechanical properties of this alloy in the rolling direction are: yield strength 440 MPa, ultimate tensile strength 505 MPa, Young's modulus 72.6 GPa and elongation 11.4%. Paris's law coefficient, from [26] are $C = 7.50 \ 10^{-12}$ SI, $m = 4.175$ and the stress intensity factor range threshold is $\Delta K_{th} = 3.5$ MPa$\sqrt{m}$.

2.2. Fatigue test specimen

Prismatic specimens were prepared from the core of a 70 mm thick plate in such a way that bending stress is applied perpendicular to Long-transverse direction (TL). The geometry and dimensions of the specimens are given in Fig. 2. They have been initially machined by milling on a numerical machine. The surface was then finish on a shaper HERMES – RS55 without using lubricant. The machining conditions have been chosen from a response surface methodology in order to produce a surface roughness R_a of 0.8 μm which is a usual value for aluminum alloy aeronautical machined parts. The machining direction corresponds with the rolling direction (L). The machining conditions are given in Table 2.

2.3. Surface treatments

Specimens were categorized in three groups: in the first group, no treatment was done after machining in order to build a reference fatigue curve; the specimens of the second group were only pickled after machining and those of the third group were pickled and anodized. Anodic oxidation has been realized in a chromic acid bath by our industrial partner in order to respect industrial protocols effectively used by industry.

Before pickling process, specimens were degreased in order to produce a chemical cleaned surface. This degreasing was carried out in alkaline solution (pH = 9) at 60 °C for 3 min followed by water rinsing.

Pickling was done in two steps: a first one in a sodium solution at 32 °C followed by rinsing and the second step in an ARDROX solution at 32 °C for 3 min followed by rinsing.

Chromic acid anodization was done in anhydride chrome CrO_3 solution at 40 °C for 50 min.

Table 1
Chemical composition of 7050 aluminum alloy analysis with EDS.

Element	Cu	Mg	Mn	Si	Fe	Zn	Zr	Ti	Al
Weight (%)	1.76	2.42	0.07	0.28	0.19	6.15	0.14	0.06	Bal.
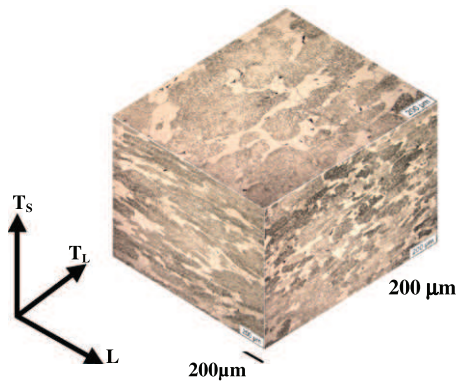
Fig. 1. Microstructure of 7050-T7451 (L = Rolling direction, TL = Transverse-long direction, TS = Transverse-short).

Fig. 2. Fatigue test specimens geometry and dimensions (all sizes in mm).

Table 2
Machining conditions.

R_a (µm)	Cutting speed (m/min)	Feed (mm/tr)	Depth of cut (mm)	Tool nose radius (mm)
0.8	180	0.1	0.5	0.8

The average thickness of oxide layer produced by this process was measured to be about 3 µm using SEM observation.

2.4. Surface topography measurements

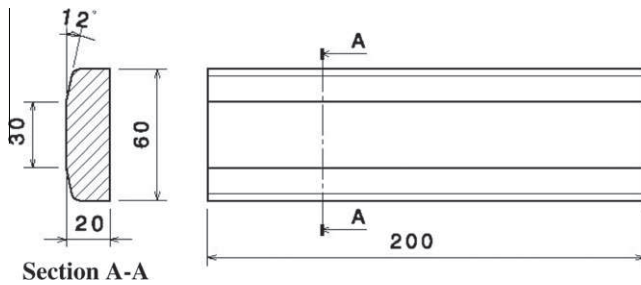Surface topography measurements were done using a Mahr PKG120 profilometer with a conical diamond stylus (60°–2 µm radius). Specimens were placed on the synchronized profilometer table such as the direction of measurement match with the applied stress direction. The resolution in this direction was chosen equal to 5 µm as well as in the transverse direction in order to reduce the data file size without missing important topography information such as pickling pits. However, this methodology limits the accuracy of pit size determination; if length and width determination of pit can be considered as sufficiently accurate, determination of depth can be flawed, in particular due to diamond stylus angle: the stylus cannot detect the real bottom of the cavity.

2.5. Fatigue tests

Specimens were tested in four-point bending fatigue on a 100 kN MTS servo-hydraulic fatigue machine at a frequency of 10 Hz at ambient temperature, under a stress ratio R of 0.1.

## 3. Experimental results

3.1. Surface topography

SEM observations of several degreased and pickled specimens showed that degreasing had no effect on surface topography. Moreover, pickling process had deleterious effects on surface: several pits have been observed (Fig. 3a). They were principally found in recrystallized grains. EDS analysis showed that these pits were due to dissolution of aluminum around intermetallic particles or to partial dissolution of these particles. No evidence of intergranular penetration was observed. Concerning anodized surface, SEM observations did not reveal any notable increase of surface degradation (Fig. 3b): on the contrary, if pickling pits size was small enough, oxide layer recovered these pits so that the number of detected pits decreased.

3.2. Fatigue tests results

The results of four-point bending fatigue test for the three surface conditions (just machined, pickled and anodized) are represented on Fig. 4. As it can be seen, anodizing leads to an important decrease of the fatigue resistance but this decrease is less important when the applied stress level increases. The essential of this decrease (90%) is caused by pickling process. The last 10% are caused by anodizing itself.

In the case of machined state, the nucleation sites of the fatigue cracks were analyzed using EDS during MEB observations. These sites were identified to be intermetallic particles Mg_2Si and Al_7Cu_2Fe [25] (Fig. 5). For low stress level, single crack was observed. Few multi cracks were observed only in the case of high stress levels.

In the case of pickled state, multiple nucleation sites were observed even for low stress levels. The nucleation sites were identified to be the pickling pits created during pickling process. These pits were created by dissolution of the inter-metallic particles rich in copper Al_7Cu_2Fe and Al_2CuMg (Fig. 6). The mean depth of these
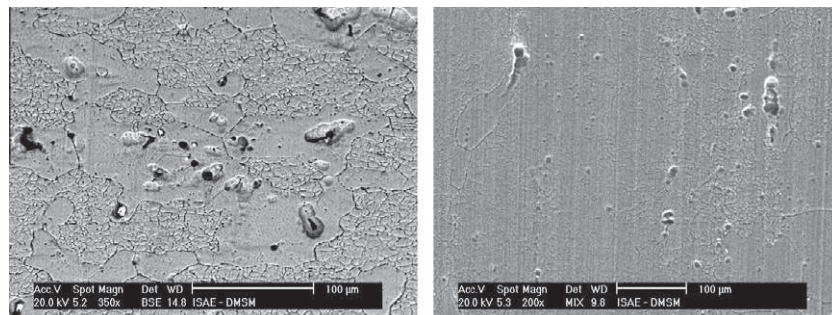
Fig. 3. MEB observation of surface of 7010-T7451 specimen after (a) pickling process and (b) anodic oxidation process.
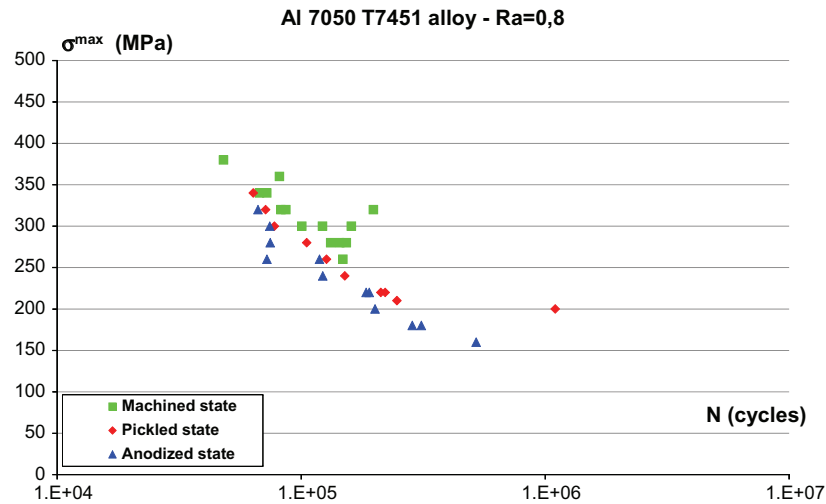
Fig. 4. Fatigue results for Al7050-T7451 alloy in four-point bending, for machined roughness R_a of 0.8 mm, for the three states of surface: machined, pickled and anodized.
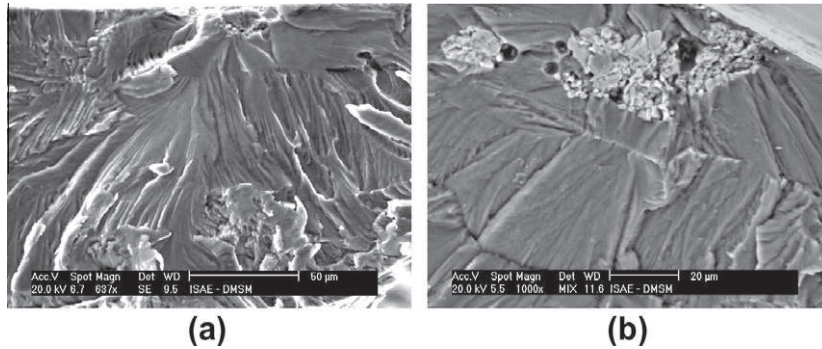

Fig. 5. Crack nucleation sites for machined condition: intermetallic particles (a) Mg_2Si – (b) Al_7Cu_2Fe.
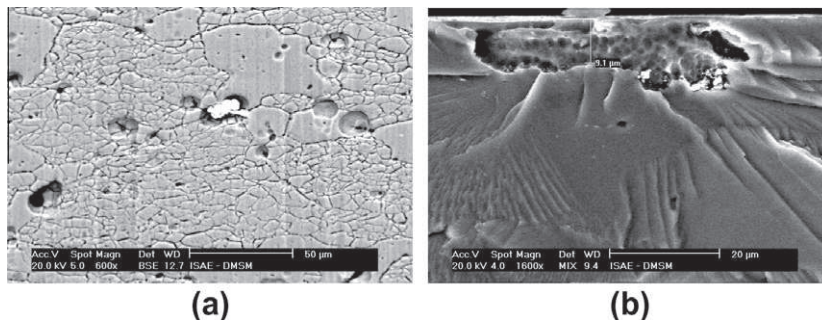
Fig. 6. Pickling pits on surface (a) as crack nucleation sites for pickled state (b).

nucleation pits was about 8 μm. Coalescence of neighboring cracks was equally observed.

In the case of anodized specimens, surface observations revealed that the oxide layer was able to cover pickling pits of small size. On the contrary, the size of the larger pickling pits increased during oxidation process. In that case, fatigue cracks nucleated from these pits (Fig. 7).

4. Modeling

In order to predict fatigue life of pickled and anodized 7050 alloy, an analytical model has been developed based on linear fracture mechanics with plasticity correction. This model is based on Suratchaï's model in which surface roughness is considered as stress concentrator [20]. In Suratchaï's model, a 2D finite elements model of the surface, built from experimental roughness profile, allows calculating a stress concentration coefficient. With an initial crack length equal to the mean size of recrystallized grains (preferential initiation sites), it is then possible to predict fatigue life time by iterative calculation of fatigue crack propagation rates and crack length.

Even if fatigue crack initiation mechanisms were the same for machined and pickled or anodized ones, initial Suratchaï's model was not able to correctly predict fatigue life for pickled and
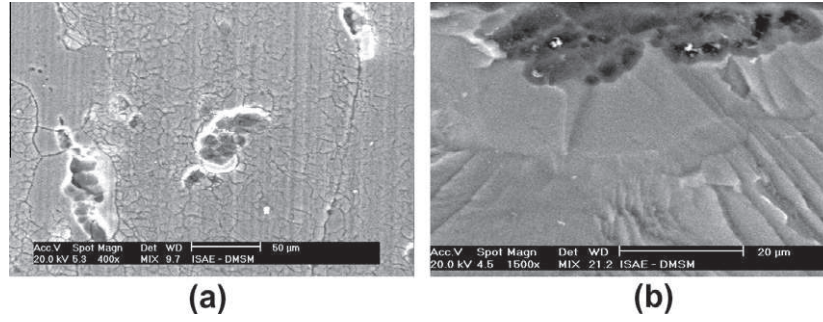
Fig. 7. Pickling pits on surface (a) as crack nucleation sites for anodized state (b).

anodized conditions: it largely overestimated fatigue life. In the presented model, and in order to make better predictions each pit was considered as a semi-elliptical flaw (depth a_i, length along transverse direction c_i) from which micro-crack could nucleate if stress intensity factor range was high enough. Surface stress intensity factor was calculated considering stress concentration induced by machining roughness. Stress intensity factor range through the depth was calculated considering stress concentration effect of pickling pits while cracks could be considered as short cracks. Two crack propagation stages were also considered; the first one, a short crack growth rate law was used in order to take into account the very low size of the initial cracks (pits) and to take into account a higher growth rate comparing to long cracks at the same stress intensity factor range. The second one was the long crack growth law of Paris–Erdogan. The both used crack growth laws implicitly included the influence of microstructure and internal stress state on crack propagation whatever the stage was. Multi cracking and coalescence were considered too. Crack propagation was calculated simultaneously at the surface and through the depth of the specimen.
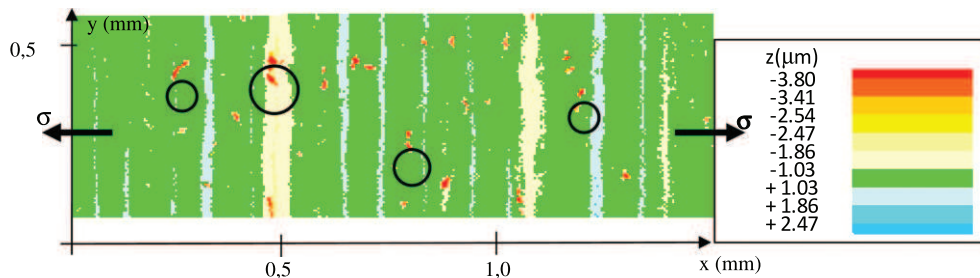
4.1. Pits characterization

Pits characterization was realized from the surface topography: after a plane correction using least square method, data were scanned. One current point was assumed to belong to one pit if the following condition was verified

$$z_{ij} < R_a \tag{1}$$

where z_{ij} represented the measured depth and R_a the average roughness measured using roughness profiles

$$R_a = \frac{1}{l} \int_0^l |z(x)| dx \tag{2}$$

Then, all the adjacent points for which the above condition was respected were assumed to belong to the same pit. Fig. 8 gives an example of such characterization: some pits are identified with circles.

With this tool, each pit can be characterized not only by its maximum depth, its length (along transverse direction y) and width (along applied stress direction x) but also by its position at the surface. The size of the chosen diamond stylus led to a lack of accuracy in the pit sizing: some sever shape could have been underestimated. Several 2×2 mm areas at the surface were measured in order to obtain a statistical analysis of pickling pits. Such statistical treatment allows establishing depth repartition graphs for pickling pits on the surface (Fig. 9).

Concerning the anodized surface topography, such tool was of no usefulness as pickling pits, for most of them, were recovered by the oxide layer. Only biggest pickling pits whose size increased during anodizing process could be characterized so that surface characterization was not representative of surface as flaws from which cracks could nucleate were not identified.

4.2. Pickling pits stress concentration coefficient calculation

To define stress concentration induced by pickling pits, finite elements model using Abaqus software© was built from surface topography. 8 nodes linear bricks have been used. The element size was defined according to the resolution used for topography measurements in each direction of the surface (Fig. 10a). The thickness of the meshed volume was chosen equal to 50 μm using 10 elements: for each column of elements, the thickness ratio was calculated from the depth of the surface point.

Displacements were applied on the extreme transverse sections along x-direction. The calculation was elastic. This model allowed calculating for each pit (i) the value of the local stress, denoted $\sigma_{i,loc}^{max}$ equal to the average value of (Fig. 10b) σ_{xx} on five elements depth corresponding to the mean size of grains in which nucleation occurred. Then, for each pit, a stress concentration coefficient Kt_i was defined as

$$Kt_i = \frac{\sigma_{i,loc}^{max}}{\sigma_{nom}^{max}} \tag{3}$$

Let remark that the effects of lack accuracy of pit sizing due to the choice of the diamond stylus were fitted by the choice of the finite elements meshing which had to be sufficiently refined to
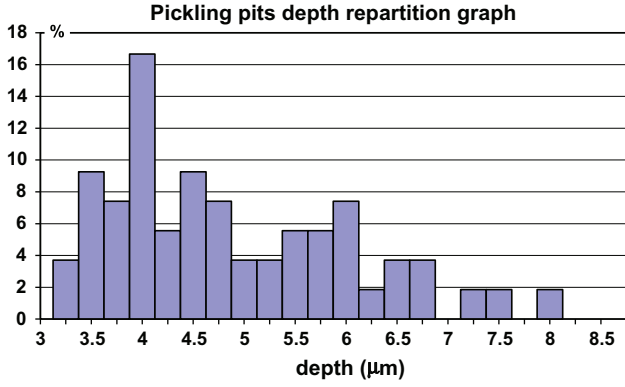

Fig. 8. Example of pickled surface topography characterization.

Fig. 9. Depth repartition graphs for pickling condition.

represent as well as possible the shape of the pits, but, on another hand, not too refined to be representative of one of the main assumption of finite element calculation: homogeneity.

4.3. Multi-crack propagation model

4.3.1. Condition of crack propagation

The condition for propagation of a crack nucleated from one pit (i) was that the stress intensity factor at the bottom of this pit is higher than the corresponding short crack stress intensity threshold $\Delta K_{th,a_i}$

$$If \quad \Delta K_{a_i} \leqslant \Delta K_{th,a_{0i}} \quad then \quad no\ propagation \tag{4}$$

The short crack stress intensity threshold $\Delta K_{th,a_i}$ was calculated using Santu's model [27]

$$\Delta K_{th,a_i} = \Delta K_{th} \cdot \sqrt{\frac{a_0}{a_0 + a_{0_i}}} \tag{5}$$

where a_0 corresponds to the maximum length of long cracks which do not propagate under fatigue limit stress σ_D; this length a_0 was calculated using *El* Haddad's relation [28]

$$a_0 = \frac{1}{\pi} \cdot \left(\frac{\Delta K_{th}}{(1-R) \cdot \sigma_D} \right)^2 \tag{6}$$

where ΔK_{th} is the threshold for long cracks defined for the same stress ratio as used for the fatigue test.

4.3.2. Crack propagation model

When cracks nucleate from pits, they are short cracks and their growth rate is higher than the growth rate of long cracks, even for the same stress intensity factor range [29]. The short crack propa-

gation stage depends on microstructure and stress level. In some conditions, shorts cracks can even stop when they reach a microstructural barrier [30]. If mechanisms of propagation of short cracks are better known, few models are available [31,32,27]. Unfortunately, no experimental data were available to identify a short crack growth rate law so that, in the present study, a simple model has been used: cracks for which crack propagation condition is respected (relation (4)) are supposed to propagate first with a constant growth rate (short crack propagation stage) until their length become long enough to propagate under Paris's law (long crack propagation stage). This model is not able to integrate microstructural considerations or internal stress state.

The short crack growth rate was chosen equal to the value of the crack growth rate corresponding to the long crack threshold ΔK_{th}, using Paris' law

$$\left. \frac{da}{dN} \right|_{fc,a_{0i}} = C \cdot (\Delta K_{th})^m \tag{7}$$

where C and m represents the material coefficient of Paris' law.

It is independent from initial flaw size.

For the propagation through the depth, during the short crack propagation stage, it was supposed that the stress concentration generated by the presence of one pit influences stress intensity factor at the bottom of the crack nucleated from a pit (i) and that this stress concentration was predominant on geometric factor:

$$\Delta K_{a_i} = (Kt_{a_i} \cdot \Delta\sigma) \cdot \sqrt{\pi a_i} \quad while \ \Delta K_{a_i} \leqslant \Delta K_{th} \tag{8}$$

After the stress intensity factor reached the long crack threshold, no more influence of stress concentration was considered and crack shape influence was reconsidered, so that the stress intensity factor at the tip of the crack was equal to

$$if \ \Delta K_{a_i} > \Delta K_{th} \quad then \quad \Delta K_{a_i} = F_{a_i} \cdot \Delta\sigma \cdot \sqrt{\pi a_i} \tag{9}$$

In relation (8) and (9), a_i represents the current depth of the crack i, and $\Delta\sigma$ the stress range; in relation (8), Kt_{a_i} represents the stress concentration factor at the bottom of the pit.

On the other hand, it was considered that, whatever the propagation stage, the propagation at the surface was always influenced by the surface roughness which acts as stress concentrator. This assumption implies that damaging pits are supposed to be localized at the bottom of the machining striation. Consequently, the calculation of the stress intensity factor was modified by integrating the roughness stress concentration coefficient

$$\Delta K_{surf} = F_{C_i} \cdot Kt_{surf} \cdot \Delta\sigma \cdot \sqrt{\pi c_i} \tag{10}$$

where c_i represents the half length of the crack, $\Delta\sigma$ the stress range and Kt_{Surf} the machining roughness stress concentration coefficient
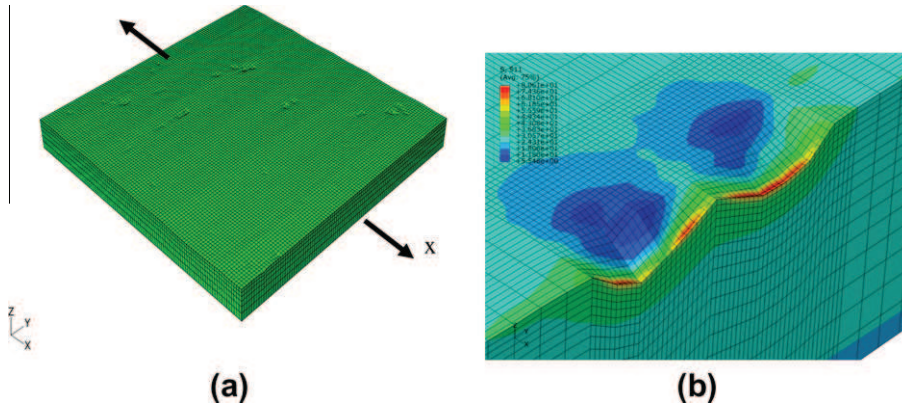

Fig. 10. Example of finite elements model built from surface topography – meshed volume (a) and detail of results (b).

which was calculated from roughness profile measurements on machined state using Suraratchaï's method [20].

In these above expressions (Eqs. (6), (7), and (9)) of the stress intensity factor, F_{a_i} and F_{c_i} represent the geometric factor respectively at the bottom of the semi-elliptical crack and at the surface tip of the crack. They depend on shape ratio a_i/c_i and are calculated using Newman–Raju's model [33].

4.3.3. Coalescence between neighboring cracks

Propagation rate of a crack is influenced by the proximity of other cracks. This influence can be taken into account through the modification of the geometric factor F in the stress intensity factor calculation. During propagation, neighbored cracks can interact even if the crack tips do not touch. At this moment, two cracks become one single crack which is not necessary semi-elliptical. Then this crack will develop to a semi-elliptical shape: it is the coalescence step. After that, the propagation of this crack continues until it interacts with another crack and so on. Several models of crack interaction have been reviewed [34]. In the present model, coalescence was considered when the plastic zones which develop at the crack tips reach one each other. The coalescence condition was expressed as follows

$$d_{ij} \leqslant zp_i + zp_j \qquad (11)$$

where d_{ij} represents the distance between the tips of the two cracks i and j, and zp_i and zp_j the plastic zone diameter of these two cracks.

When two cracks coalesce, the length of the new crack is defined equal to the sum of the lengths of these two cracks, including the plastic zones, and the depth is equal to the maximum of the depth of the two cracks. This is represented by the dotted ellipse in Fig. 11.

4.3.4. Anodized coating

SEM observations of oxide layer and transversal sections of specimens showed that pickling size increased only for previously large pits. But for smaller ones, it was observed that the oxide layer recovered these pits without suppressing them; flaws were still present. During surface topography measurements, these recovered pits could not be detected and then sized using the presented above method (see Section 4.1). As the fatigue life model is built on measured surface topography, it is clear that, in the case of anodized conditions, it will give under-estimated predictions as only few biggest pits were characterized, which were not necessary the most deleterious pits from fatigue point of view.

On another hand, from experimental SEM observations of tested specimens, there was no evidence of coating crack initiating from external surface so that it was assumed that fatigue cracks initiated from pickling pits. As it is generally assumed oxide layer has a brittle behavior and so is subjected to quite instantaneously cracking [4,6,7]. Such behavior leads to instantaneous increase of the lengths of the cracks which nucleate from pits, and thus affects short crack propagation stage. This assumed mechanism was introduced in the present model by increasing arbitrarily the size of all the pits.

$$a_{0i} = a_{0i} + e \qquad (12)$$

where e represents the thickness of the oxide layer; in our case, $e = 3$ μm.

Simultaneously, the length and the width of the pits at the surface were equally increased in order to keep the same aspect ratio, as it has been observed on anodized surface.

5. Simulations results and discussion

Previously to any crack propagation simulation, EF simulation were made in order to calculate the stress concentration coefficients for each pit location (Fig. 12a). As well as for pits characterization, the simulations of several cases allowed establishing a repartition graph of the stress concentration coefficient for pickled conditions (Fig. 12b). This graph shows the influence of the pits considering the pits surface repartition. This graph gives good information on the surface degradation according to fatigue behavior if one considers that roughness is the principal influence factor on fatigue life.

Simultaneously, the machining roughness stress concentration coefficient Kt_{surf} was evaluated to 1.08 using Suraratchaï's model [20] with several profiles roughness.

In order to show the importance of the different hypotheses used in this model, two analytical simulations were made. In the first analytical one, called ML model (Multicrack-Long crack stage), no small crack propagation stage was introduced so that, as soon as cracks nucleated from pits, i.e. crack condition was respected (relation (4)), they were considered as long cracks and the propagation was calculated using Paris' law. During the propagation calculation process, coalescence condition was verified at each calculation step between each propagating cracks.

Then, in the second analytical simulation, called MLS model (Multicrack + Long crack stage + Short crack stage), a short crack stage was considered. This short crack stage was characterized, for each crack nucleating from each pit, by a constant growth rate which was defined from the long crack threshold (Eq. (7)).

The fatigue life predictions given by these two models (ML and MLS) in the case of pickled state are illustrated in Fig. 13. As it can be seen, if predictions given by the two models can be considered as in good agreement with experimental data, fatigue life predictions given by the ML model are over estimated. This means that the only consideration of multi cracks is not sufficient to represent fatigue behavior of pickled surface even when stress concentration effect at pit's location is considered. On the contrary, taking into account the short crack stage gives conservative predictions comparing to experimental results. Such results have been observed for 7010 pickled specimens [23].

To the author's opinion, the remaining differences which can be observed are certainly due to the model of the short crack propagation stage and prove that this aspect is very important and has to be studied in future works.

The complete model was applied to the anodized state. In that case, the presence of the oxide layer was taken into account
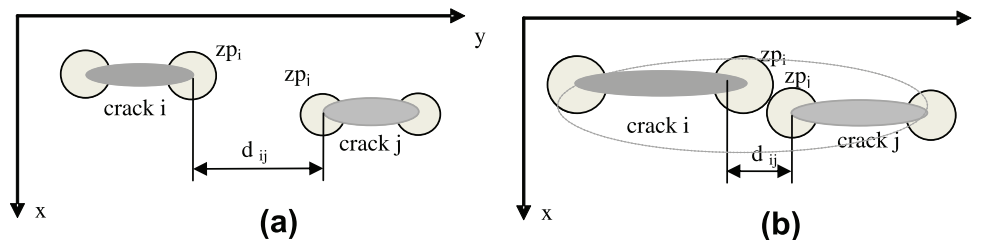

Fig. 11. Schema of coalescence calculation (a) before coalescence – (b) condition of coalescence (dotted ellipse = coalesced crack).
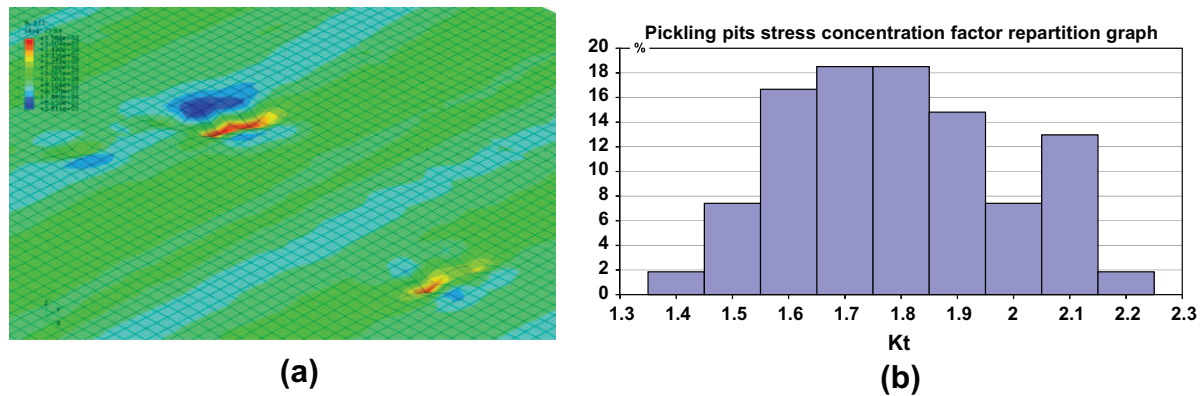
Fig. 12. Examples of results of finite elements model (a) and repartition graph of concentration coefficient (b) for a pickled surface.
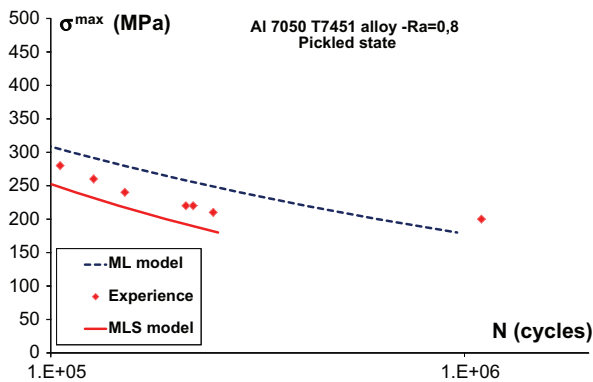

Fig. 13. Experimental results and predictions given by the ML and the MLS models for the pickled condition.
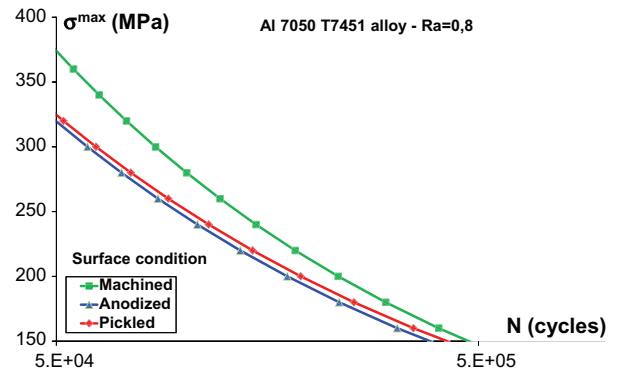

Fig. 15. Experimental results for machined condition and prediction for the pickled and anodized conditions.

through the increase of the depth of the pits which were responsible for crack nucleation. The predictions for anodized conditions are shown in Fig. 14. As it can be observed, predictions are also in good agreement with the experimental results.

On Fig. 15, the predictions given by the complete model for the three surface conditions, machined, pickled and anodized, are gathered. For machined condition, the fatigue curve is the experimental results fit curve. It appears clearly that the complete model, integrating multi cracking and short crack growth rate is able to describe the decrease induced by the two steps of anodizing process and respect the respective influence of each step of the
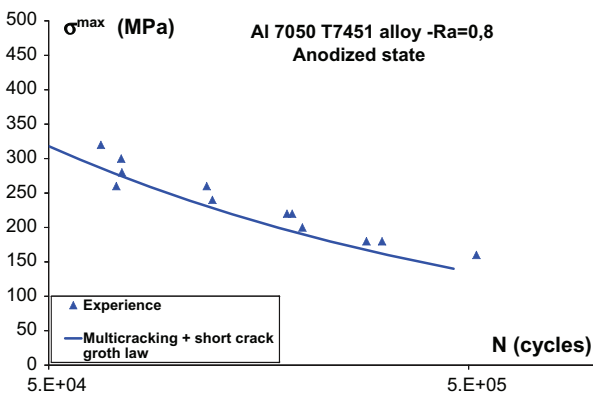

Fig. 14. Experimental results and predictions given by the complete model for the anodized condition.

process. However, if this complete model gives suitable results, the part of decrease obtained for the pickled condition is slightly too important relatively to the decrease corresponding to anodization, when compared to experimental results for which it was observed that about 90% of the total decrease was caused by pickling process and the last 10% by anodizing process. This can be explained by the lack of accuracy in the description of the topography and for a great part in the too simple nature of the short crack growth law.

On another hand, under-estimation of pickling process effect (Fig. 12) is balanced with an over-estimation of the oxide layer effect. This over-estimation in the case of anodized conditions can be also explained by the choice of the short crack growth law. The instantaneous increase of the depth of the flaws affect the number of cycles under short crack propagation stage and thus the number of cycles before short crack and long crack transition. To the opinion of the author, adjustment of the short crack growth is necessary and will be one of the investigation ways for the future.

6. Conclusion

The decrease of fatigue life observed after chromic acid anodizing process in case of 7050 aluminum alloy was principally caused by pickling step prior to anodizing one. The pickling operation led to formation of pits by dissolution of intermetallic particles at the surface or by dissolution of the aluminum matrix around the particles which caused the ejection of these particles. Whatever the reason of the pit formation, these pits acted as stress concentrator and promoted the nucleation of many small cracks. In order to

predict fatigue life of anodized 7050 aluminum alloy parts, a propagation model has been developed. This model included multi cracking process and a short crack growth stage. The pickling pits which were responsible for crack nucleation were considered as stress concentrator: they influenced the stress intensity factor and thus the crack growth of short cracks. The stress concentration coefficient at the bottom of each pit was calculated using a finite elements model built from pickled surface topography measurements. During their propagation, neighboring cracks, even if they are short cracks, can coalesce. This phenomenon was also included in the proposed model. Nucleation condition depended on pit size: it was assumed to occur if stress intensity factor range was higher than a short crack threshold which was assumed to depend on pit size. The short crack growth rate was calculated using Paris' law for long crack threshold: it did not depend on pit size. In the case of anodized condition, the oxide layer was taken into account by increasing the depth of the pickling pits. Simultaneously, length and width at the surface were also increased to keep the same aspect ratio. Comparison between modeling results and experimental data obtained in four point bending fatigue tests on as machined, pickled and anodized conditions showed a good agreement. Predictions were conservatives for pickled conditions; this can be explain by the several assumptions which were used in the model, in particularly concerning in the definition of the short crack growth law which is largely too simple due to lack of accuracy. Another explanation concerns the lack of accuracy of pit size characterization which flawed estimation of short crack propagation stage.

Acknowledgment

References

[1] ASM Handbook. Corrosion, vol. 13. USA: ASM International; 1992.
[2] Cree AM, Weidmann GW. Effect of anodized coatings on fatigue cracks rates of aluminium alloy. Surf Eng 1997;13(1):51–5.
[3] Kermanidis AL, Th, Petroyiannis PV, Pantelakis Sp. G. Fatigue damage tolerance behaviour of coroded 2024 T351 aircraft aluminium alloy. Theorical and Applied Fracture Mechanics 2005;43:121–32.
[4] Lonyuk B, Apachitei I, Duszczyk J. The effect of oxide coatings on fatigue properties of 7475-T6 aluminium alloy. Surf Coat Technol 2007;201(21):8688–94.
[5] Sadeler R. Effect of a commercial hard anodizing on the property of a 2024-T6 aluminium alloy. J Mater Sci 2006;41:5803–9.
[6] Camargo A. Voorwald, Influence of anodization on the fatigue strength of 7050-T7451 aluminium alloy. Fatigue Fract Eng Mater Struct 2007;30:993–1007.
[7] Cyrik E, Genel K. Effect of anodic oxidation on the fatigue performance of 7075-T6 alloy. Surf Coat Technol 2008;202:5190–201.
[8] Shahzad M, Chaussumier M, Chieragatti R, Mabru C, Rezaî-aria F. Effect of sealed anodic film on fatigue performance od 2214-T6 aluminium alloy. Surf Coat Technol 2012;206:2733–9.
[9] Rokhlin SI, Kim JY, Nagy H, Zoofan B. Effect of pitting on fatigue crack initiation and fatigue life. Eng Fract Mech 1998;62:425–44.
[10] Pao PS, Gill SJ, Feng CR. On fatigue crack initiation from corrosion pits in 7075-T7351 aluminium alloy. Scripta Mater 1998;43(5):391–6.
[11] Dolley EJ, Wei RP. The effect of pitting corrosion on fatigue life. Fatigue Fract Eng Mater Struct 2000;23:555–60.
[12] Rateick RG, Griffith RJ, Hall DA, Thompson KA. Relationship of microstructure to fatigue strength loss in anodized aluminium–copper alloys. Mater Sci Technol 2005;21:1227–35.
[13] Thompson GE, Zhang L, C. Smith JE, Skeldon P. Boric/sulfuric acid anodizing of aluminum alloys 2024 and 7075: film growth and corrosion resistance. Corros Sci 1999;55:1052–60.
[14] Snogan F, Blanc C, Mankowski G, Pébère N. Characterisation of sealed anodic films on 7050 T74 and 2214 T6 aluminium alloys. Surf Coat Technol 2002;154:94–103.
[15] Liu JH, Li M, Li SM, Huang M. Effect of the microstructure of Al 7050-T7451 on anodic oxide formation in sulfuric acid. Int J Mineral, Metal Mater 2009;16:432–8.
[16] Barter SA. Fatigue crack growth in 7050 aluminium alloy thick section plate with a surface condition simulating some regions of F/A-18 structure, DSTO-TR-1458, 2003.
[17] Isida M, Yoshida T, Noguchi H. Tension of a finite-thickness plate with a pair of semi-elliptical surface cracks. Eng Fract Mech 1990;35(6):961–5.
[18] Murakami Y, Nemat-Nasser S. Interacting dissimilar semi-elliptical surface flaws under tension and bending. Eng Fract Mech 1982;16(3):373–86.
[19] Chieragatti R, Surarachai M, Mabru C, Espinosa C, Vergnes V. Procédés de caractérisation de la tenue en fatigue d'une pièce à partir de son profil de surface. French Patent no 0650793, 2006.
[20] Suraratchaï M, Limido J, Mabru C, Chieragatti R. Modelling the influence of machined surface roughness on the fatigue life of aluminium alloy. Int J Fatigue 2008;30(12):2119–26.
[21] Shahzad M, Chaussumier M, Chieragatti R, Mabru C, Rezaï-Aria F. Influence of surface treatments on fatigue life of Al 7010 alloy. J Mater Process Technol 2010;210(13):1821–6.
[22] Shahzad M, Chaussumier M, Chieragatti R, Mabru C, Rezaï-Aria F. Influence of anodizing process on fatigue life of machined aluminium alloy. Procedia Eng 2010;2(1):1015–24.
[23] Chaussumier M, Shahzad M, Mabru C, Chieragatti R, Rezaï-Aria F. A fatigue multi-site cracks model using coalescence, short and long crack growth laws, for anodized aluminum alloys. Procedia Eng 2010;2(1):995–1004.
[24] Chieragatti R, Espinosa C, Lacome JH, Limido J, Mabru C, SALAUN M. Influence of roughness on the fatigue of machined surfaces: determination of local stress concentration. 29èmes journées de Printemps, JP 2010 2010. 19–20 May 2010.
[25] Shahzad M, Chaussumier M, Chieragatti R, Mabru C, Rézaï-Aria F. Surface characterization and influence of anodizing process on fatigue life of 7050 alloy. Mater Des 2011;32(6):3328–35.
[26] Przystupa MA, Bussi RJ, Magnusen PE, Hinkle AJ. Microstructure based fatigue life predictions for thick plate 7050-T7451 airframe alloy. Int J Fatigue 1997;10(1):285–8.
[27] Santus C, Taylor D. Physically short crack propagation in metals during high cycle fatigue. Int J Fatigue 2009;31:1356–65.
[28] Haddad MH, Topper TH, Smith KN. Prediction of non propagating cracks. Eng Fract Mech 1979;11(3):573–84.
[29] Pearson S. Initiation fatigue cracks in commercial aluminium alloys and the subsequent propagation of very short cracks. Eng Fract Mech 1975;7(2):235–47.
[30] Lankford J. The influence of microstructure on the growth of small fatigue cracks. Fatigue Fract Eng Mater Struct 1895;8:161–75.
[31] Newman JC, Philipps EP, Swain MH. Fatigue life prediction methodology using small-crack theory. Int J Fatigue 1999;21:109–19.
[32] Chapetti MD. Fatigue propagation threshold of short cracks under constant amplitude loading. Int J Fatigue 2003;25:1319–26.
[33] Newman JC, Raju IS. Stress-intensity factor equations for cracks in three dimensional finite bodies subjected to tension and bending loads. In: ATLURI SN, editor. Computational methods in mechanics of fracture. Elsevier Science Publishers; 1986. p. 312–34.
[34] DeBartolo EA, Hillberry BM. A model of initial flaw sizes in aluminium alloys. Int J Fatigue 2001;23:79–86.